Gamma-ray Image Noise Generation Using Energy-Image Converter Based on Image Histogram

Ren Komatsu[1], Hanwool Woo[2], Yusuke Tamura[3], Atsushi Yamashita[1], and Hajime Asama[1]

***Abstract*— We propose a novel method to simulate image noise caused by gamma-ray irradiation. Monte Carlo simulation is utilized to calculate the interaction between the gamma-ray and the image sensor, and the energy deposit in each pixel is estimated. A converter module is proposed for generating image noise from the energy deposit. The conversion is designed so that the converted energy deposit has a similar image histogram to the real gamma-ray image noise. The real gamma-ray image noise is obtained by using circular fisheye cameras in gamma-ray irradiation tests. We demonstrate the effectiveness of the proposed method in experiments. We believe that this study would be beneficial for the development of methods for decommissioning the Fukushima Daiichi Nuclear Power Plant by the research community. Our source code is available at `https://github.com/matsuren/pixel_noise_sim_geant4`.**

I. INTRODUCTION

On March 11, 2011, the Great East Japan Earthquake occurred, and the Fukushima Daiichi Nuclear Power Plant (FDNPP) was damaged by the tsunami following the earthquake. As a result, Units 1, 2, and 3 of the FDNPP experienced core meltdowns, and Units 1, 3, and 4 experienced hydrogen explosions. It is estimated that the decommissioning of FDNPP would take 30–40 years to complete [1]. Because of the high radiation resulting from core meltdowns and explosions, many places in FDNPP are dangerous for humans. Therefore, robot teleoperations have been utilized for the decomissioning [2], [3]. Moreover, the demand for robot teleoperations will increase even further in the next decommissioning stage, which is expected to involve fuel debris retrieval in the reactor pressure vessels (RPVs) where extremely high levels of radiation exposure are expected in the approach to the fuel debris.

In robot teleoperation, an operator controls a robot remotely from a control room safely while viewing images captured by the cameras mounted on the robot. Hence, the operator plays a critical role in deciding the next movement of the robot based on the captured images. Therefore, it is beneficial if the operator can practice controlling robots in environments similar to FDNPP. The Japan Atomic Energy Agency operates the Naraha Center for Remote Control Technology Development, where there are full-scale mockups of the stairs in FDNPP for robot teleoperation training [4]. In addition, Suzuki et al. developed a simulated environment of the primary containment vessels (PCVs) of Units 1, 2, and 3 in FDNPP [5]. Operators can control robots in the simulated environment for training utilizing a dynamics simulator for robots called Choreonoid [6].

However, the operators should also be prepared for the effects of gamma-ray irradiation on the image sensors when they control robots in high-radiation environments such as the PCV or RPV in FDNPP. The main effects of gamma-ray irradiation are camera malfunctions and image noise. Without proper knowledge of the gamma-ray effects, the operators may be surprised by sudden camera malfunctions during operation. In addition, gamma-ray image noise makes the captured images difficult to interpret, which may cause an additional burden on the operators if they are not used to the appearance of image noise. Furthermore, image noise can deteriorate the performance of localization and mapping algorithms which help the operators to understand the surrounding environment. To study camera malfunctions, Nagatani et al. and Komatsu et al. conducted gamma-ray irradiation tests and found that the cameras failed at the total dose of 141.3–224.1 Gy [7], [8]. To study the image noise, Lee et al. conducted gamma-ray irradiation tests and investigated the effects of image noise on localization and mapping algorithms [9]. Real gamma-ray irradiation was utilized in the irradiation tests in these studies; however, the gamma-ray irradiation tests are costly and require specific facilities. Therefore, it is difficult to conduct gamma-ray irradiation tests for training robot teleoperation operators.

In this study, we propose a novel method to simulate image noise caused by gamma-ray irradiation. Because camera malfunction can be reproduced easily by estimating the total dose on the cameras, we focus on the image noise. Monte Carlo simulations are performed to calculate the interaction between the gamma-ray and the image sensor and the energy deposit in each pixel is estimated. Moreover, we propose a converter module utilizing image histogram comparison for converting the energy unit of electron volts (eV) in each pixel to the pixel intensity to generate image noise. Finally, the effectiveness of the proposed method is demonstrated by experimental results.

The proposed method would be beneficial not only for training robot teleoperation operators but also for researchers

*A part of this study is financially supported by the Nuclear Energy Science & Technology and Human Resource Development Project (through concentrating wisdom) from the Japan Atomic Energy Agency / Collaborative Laboratories for Advanced Decommissioning Science.

[1]R. Komatsu, A. Yamashita, and H. Asama are with the Department of Precision Engineering, Graduate School of Engineering, The University of Tokyo, Tokyo 113-8656, Japan (email: {komatsu, woo, yamashita, asama}@robot.t.u-tokyo.ac.jp).

[2]H. Woo is with the Institute of Engineering Innovation, Graduate School of Engineering, The University of Tokyo, Tokyo 113-8656, Japan (email: woo@robot.t.u-tokyo.ac.jp).

[3]Y. Tamura is with the Department of Robotics, Tohoku University, Sendai 980-8579, Japan (email: y.tamura@srd.mech.tohoku.ac.jp).

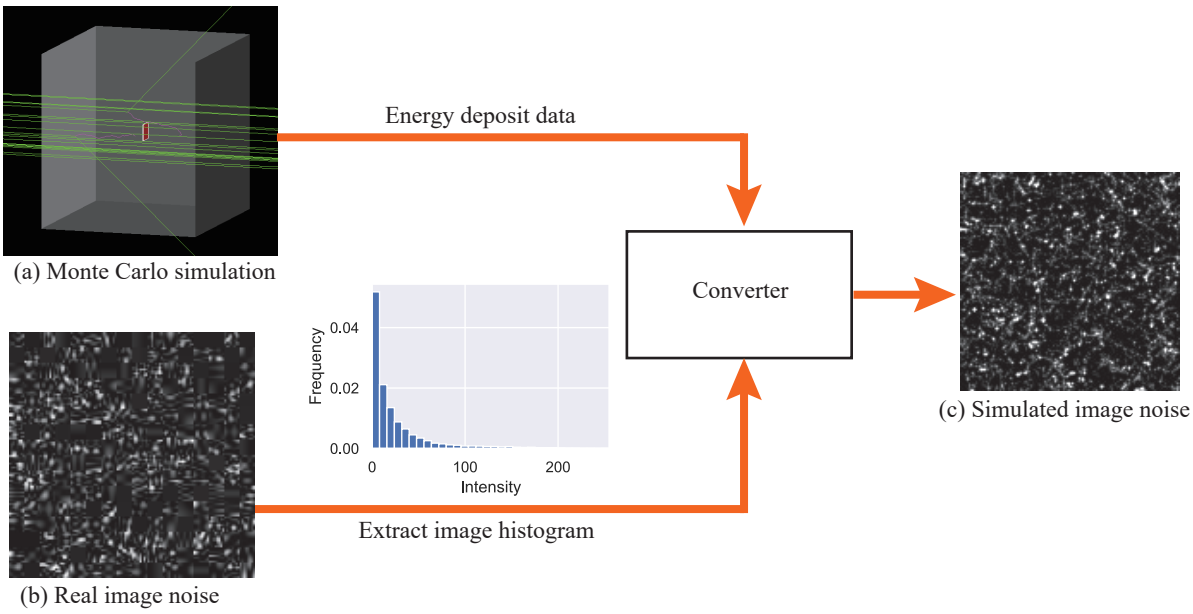

Fig. 1. Overview of proposed method. (a) Monte Carlo simulation to estimate the energy deposit in the image sensor. The red and gray boxes at the center of the figure represent the image sensor and the camera body, respectively. The green and magenta lines illustrate gamma-ray and beta-ray, respectively. (b) Real image noise obtained by the gamma-ray irradiation test. The image histogram is extracted and used to convert the energy deposit in the image sensor into simulated image noise. (c) Simulated image noise generated by the proposed method.

to develop methods for decommissioning FDNPP. For instance, Qiao et al. proposed a reconstruction method for the Unit 3 PCV [10] based on a geometric approach. The proposed method is capable of generating many noisy images which enable researchers to utilize learning-based approaches to handle the challenges in FDNPP.

II. RELATED WORK

A. Effect of gamma-ray on image sensors

Image sensors are designed to capture photons and convert them into electronic charges. Gamma-ray is a type of photon that has much higher energy than visible light. Therefore, image sensors are sensitive to gamma-ray and can be used as simple gamma-ray measurement devices [11]. Besides, a device that has large CMOS pixels has been utilized for detecting the direction of radioactive sources [12].

There are three main interactions between gamma-ray and matter, namely, the photoelectric effect, Compton scattering, and pair production. Each interaction produces electrons that are detected in the image sensors. The highest probability interaction depends on the gamma-ray energy emitted from the radioactive sources: low-, medium-, and high-energy gamma-ray mainly cause the photoelectric effect, Compton scattering, and pair production, respectively. The main interaction in radioactive sources produced in the FDNPP accident such as Cobalt-60 (^{60}Co) (0.66 MeV of gamma ray) and Cesium-137 (^{137}Cs) (1.17 MeV and 1.33 MeV) is Compton scattering.

B. Image noise simulator

The simulator developed by Suzuki et al. has a function to simulate image noise. However, they did not consider the interaction between the gamma-ray and image sensors. The image noise was simulated simply by adding random values to the images [5]. Moreover, the noise level is defined by the users. Therefore, it is difficult to simulate the noise in specific given environments, for example, simulated noise when 10 TBq of ^{60}Co is placed 1 m away from the image sensor.

In this study, we utilize Monte Carlo simulation to simulate the interaction between the gamma-ray and the image sensor. Therefore, our method is capable of simulating the image noise in given environments. Moreover, we utilize real gamma-ray image noise, which enables the proposed method to generate more realistic images.

III. METHOD

A. Overview

The proposed method generates simulated gamma-ray image noise by utilizing Monte Carlo simulation and image histogram comparison. It should be noted that we only consider 8-bit grayscale images in this study. The consideration of color images is left as a future work. An overview of the proposed method is illustrated in Fig. 1.

As shown in Fig. 1(a), a Monte Carlo simulation is first utilized to estimate the energy deposit in the image sensor. In this process, we estimate the amount of energy accumulated in each pixel during one frame of the camera.

The real image noise is then obtained in a gamma-ray irradiation test, as shown in Fig. 1(b). The image histogram is extracted from the real image noise, and the histogram is used for parameter optimization to convert the energy deposit in the image sensor into simulated image noise. In this study, the conversion is designed so that the converted

energy deposit has a similar image histogram to the real gamma-ray image noise.

Finally, as shown in Fig. 1(c), the optimized parameters are used to convert the energy deposit data into simulated image noise. It is worth noting that once the parameters are optimized, the proposed method is capable of generating noisy images from any images without noise in arbitrary environments with, for example, arbitrary radioactive sources and camera positions. Thus, an infinite number of simulated noisy images can be generated without any additional gamma-ray irradiation tests.

B. Monte Carlo simulation

1) Software: We utilize Geant4 [13], [14] for Monte Carlo simulation to calculate the interaction between the gamma-ray and the image sensor. Geant4 is a well-known toolkit that can simulate the passage of particles through matter. In particular, the low-energy package in Geant4 [15], [16] is used because the energy of gamma-ray emitted by radioactive sources is usually smaller than 2 MeV.

To calculate the interaction between the gamma-ray and the image sensor, three elements should be defined in the simulation: the energy of the gamma-ray, the material of the image sensor, and the geometry of the camera. The energy of the gamma-ray is determined based on the decay modes of the radioactive sources. For example, the energy is 662 keV for ^{137}Cs. The material of the image sensor is set to silicon dioxide because standard CMOS and CCD image sensors are made of MOSFET. Finally, the geometry of the camera is assumed to be that of the image sensor placed inside an aluminum box representing the camera body. The image sensor consists of a $W \times H$ pixel array with the dimensions of each pixel being $l_w \times l_h \times l_d$, where W, H, l_w, l_h, and l_d represent the width and height of the image resolution, and the width, height, and thickness of each pixel, respectively.

2) Reducing the computation time: A radioactive source emits gamma-ray based on its decay modes with a uniform distribution of the gamma-ray direction. Thus, an accurate simulation should reproduce the emission of gamma-ray from the radioactive source in every direction. However, the size of the image sensor is normally much smaller than the distance between the radioactive source and the image sensor. As a result, most of the gamma-ray does not affect the image sensor.

Therefore, the proposed method considers the emission of parallel beams of gamma-ray to the image sensor to decrease the required number of gamma-ray emissions in the simulation in order to reduce the computation time. When A [Bq] of radioactive source is placed d [m] from an image sensor, the required number of gamma-ray emissions to simulate the image noise in one frame is formulated as follows:

$$N_{\mathrm{sim}} = \frac{AN_{\mathrm{decay}}}{N_{\mathrm{fps}}} \cdot \frac{W_{\mathrm{beam}} H_{\mathrm{beam}}}{4\pi d^2}, \tag{1}$$

where N_{decay} and N_{fps} are the number of gamma-ray beams per disintegration (e.g., $N_{\mathrm{decay}} = 2$ for ^{60}Co) and the frame rate of the camera, respectively. We utilize a $W_{\mathrm{beam}} \times H_{\mathrm{beam}}$ rectangular distribution of parallel gamma-ray beams. When the parallel beams are vertical to the image plane, W_{beam} and H_{beam} can be assigned as $Wl_w + l_{\mathrm{off}}$ and $Hl_h + l_{\mathrm{off}}$, respectively. Here, l_{off} is the offset distance to simulate the scattered gamma-ray. Reducing the computation time is paramount, especially for simulating high-dose environments with radioactive sources on the order of PBq ($= 10^{15}$ Bq) which might take a few weeks without the proposed method.

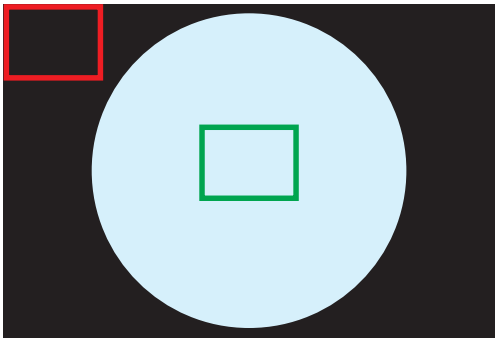

Fig. 2. Circular fisheye camera image. In the red rectangle, no scenery is captured; therefore, only gamma-ray noise can be obtained. Meanwhile, the scenery with gamma-ray noise can be captured in the green rectangle.

3) Accumulated energy deposit: Using Monte Carlo simulation, the accumulated energy deposit in each pixel is estimated. The procedure is summarized in Algorithm 1. As shown in Algorithm 1, the accumulated energy deposit during one frame of the camera is obtained as a $W \times H$ array, $V_{\mathrm{gamma}}[\cdot] = \{x \in \mathbb{R} \mid 0 \leq x\}$.

C. Collection of real image noise

The energy deposit obtained in Sec. III-B has the unit of eV; therefore, the conversion between eV and pixel intensity is required. In this study, the conversion is implemented so that the converted energy deposit has a similar image histogram to the real gamma-ray image noise. In this subsection, we describe how to obtain the real gamma-ray image noise.

Algorithm 1: Energy deposit estimation

Data: Radioactive material S
Data: Number of gamma-ray emissions N_{sim}
Result: Energy deposit in image sensor V_{gamma}
// Initialize V_{gamma} with $W \times H$ zero array
$V_{\mathrm{gamma}}[\ldots] \leftarrow 0$;
for $i \leftarrow 1$ **to** N_{sim} **do**
  // Energy based on radioactive source
  $E_{\mathrm{gamma}} \leftarrow$ `GetGammaEnergy(`S, i`)`;
  // Monte Carlo simulation
  $\{\mathcal{E}_{\mathrm{dep}}\} \leftarrow$ `SimulateGammaRay(`E_{gamma}`)`;
  foreach $\{E, h, w\} \in \mathcal{E}_{\mathrm{dep}}$ **do**
    // Accumulate deposit energy in pixel
    $V_{\mathrm{gamma}}[h, w] \leftarrow V_{\mathrm{gamma}}[h, w] + E$;
  end
end
return V_{gamma};

The real image noise is obtained in a gamma-ray irradiation test on cameras. Unlike visible light, gamma-ray can penetrate matter easily because of its high energy. Thus, Tith et al. proposed the detection of gamma-ray using smartphones, where the camera lens was covered with black tape so that only the gamma-ray but not the scenery was captured [11]. In this study, circular fisheye cameras are utilized to obtain the image noise caused by gamma-ray irradiation. Circular fisheye cameras are fisheye cameras with a field of view (FoV) of approximately 180°. Because of the super-wide FoV, the captured scenery is projected onto the image plane in a circle, and no scenery is captured outside of the circle as shown in Fig. 2. In other words, both only gamma-ray noise (the red rectangle in Fig. 2) and image with noise (the green rectangle in Fig. 2) can be captured in a single image. Here, the region where only gamma-ray noise is captured is utilized for calculating the image histograms. Meanwhile, the region of the image with noise is utilized for evaluating the proposed method.

D. Conversion between eV and pixel intensity

Finally, the energy deposit V_{gamma} is converted into the image pixel intensity $I[\cdot] = \{x \in \mathbb{Z} \mid 0 \leq x \leq 255\}$. We convert V_{gamma} into I so that the converted energy deposit has a similar image histogram to the real gamma-ray image noise.

In our preliminary gamma-ray tests, we observed that the radii of the point-shape noise is not one pixel but, rather, a few pixels. Meanwhile, the Monte Carlo simulation showed that point-shape noise usually occurs in a single pixel. We attribute this discrepancy to the leakage of energy to neighboring pixels when the gamma ray interacts with a pixel in the gamma-ray irradiation process. This leakage can be handled in the Monte Carlo simulation. Therefore, in the converter module, a Gaussian blur is applied to V_{gamma} to simulate the energy leakage. Moreover, 8×8 JPEG block noise due to the high video compression was observed in the real image. Thus, JPEG compression is applied at the end of the converter module.

The converter module `Converter`, which converts V_{gamma} into the simulated noise based on the user-defined conversion parameters $\mathcal{P}$ is described in Algorithm 2. In Algorithm 2, $\texttt{GaussianBlur}(I_{\mathrm{noise}}, p_{\mathrm{sigma}})$ is a 3×3 Gaussian blur with the standard deviation p_{sigma}. Besides, $\texttt{Compression}(I_{\mathrm{noise}}, p_{\mathrm{quality}})$ is a function that adds compression noise by applying JPEG compression with quality p_{quality} to the image. Moreover, $\texttt{Normalize}(I_{\mathrm{noise}}, p_{\mathrm{Emax}})$ is formulated as follows:

$$\texttt{Normalize}(I_{\mathrm{noise}}, p_{\mathrm{Emax}}) = 255 \cdot \min(\frac{I_{\mathrm{noise}}}{p_{\mathrm{Emax}}}, 1). \quad (2)$$

The conversion parameter $\mathcal{P}$ is optimized using a histogram comparison between the real image noise and the simulated image noise. The cost function for the optimization is defined as follows:

$$f_{\mathrm{cost}} = \texttt{EMD}(H_{\mathrm{real}}, H_{\mathrm{noise}}(\mathcal{P})), \quad (3)$$

Algorithm 2: Converter function

Data: Energy deposit in image sensor V_{gamma}
Data: Parameters for conversion $\mathcal{P}$
Result: Simulated image noise I_{noise}
Function `Convert`(V_{gamma}, $\mathcal{P}$):
  `// Initialize` I_{noise} `with` V_{gamma}
  $I_{\mathrm{noise}} \leftarrow V_{\mathrm{gamma}}$;
  `// Expand parameters`
  $\{p_{\mathrm{sigma}}, p_{\mathrm{Emax}}, p_{\mathrm{quality}}\} \leftarrow \mathcal{P}$;
  `// Conversion according to parameters`
  $I_{\mathrm{noise}} \leftarrow \texttt{GaussianBlur}(I_{\mathrm{noise}}, p_{\mathrm{sigma}})$;
  $I_{\mathrm{noise}} \leftarrow \texttt{Normalize}(I_{\mathrm{noise}}, p_{\mathrm{Emax}})$;
  $I_{\mathrm{noise}} \leftarrow \texttt{Compression}(I_{\mathrm{noise}}, p_{\mathrm{quality}})$;
  return I_{noise};
End Function

where the image histograms, H_{real} and H_{noise}, are formulated as follows:

$$H_{\mathrm{real}} = \texttt{Histogram}(I_{\mathrm{real}}), \quad (4)$$

$$H_{\mathrm{noise}}(\mathcal{P}) = \texttt{Histogram}(\texttt{Convert}(V_{\mathrm{gamma}}, \mathcal{P})), \quad (5)$$

and $\texttt{EMD}(\cdot)$ is the Earth mover's distance (EMD) [17] for evaluating the difference between the image histograms of the real and simulated image noise. Besides, $\texttt{Histogram}(\cdot)$ is a function that extracts the histogram from an image. The conversion parameter $\mathcal{P}$ can be optimized based on Eq. (3) using even a single real noisy image; however, multiple images containing real noise can be utilized by minimizing the mean absolute error of f_{cost}. Equation (3) is optimized using a grid search of the parameters $\mathcal{P} \in \{p_{\mathrm{sigma}}, p_{\mathrm{Emax}}, p_{\mathrm{quality}}\}$.

Finally, the simulated noisy images are generated based on the absolute noise model proposed in [9], which is formulated as follows:

$$I_{\mathrm{noisy}}[h,w] = \begin{cases} I_{\mathrm{noise}}[h,w], & \text{if } I_{\mathrm{noise}}[h,w] \geq I_{\mathrm{clean}}[h,w] \\ I_{\mathrm{clean}}[h,w], & \text{otherwise} \end{cases} \quad (6)$$

where I_{noisy} and I_{clean} are the simulated noisy image and the image without noise, respectively. It is worth noting that once the parameters $\mathcal{P}$ are obtained, the proposed method is capable of generating noisy images from any image without noise in arbitrary environments with, for example, arbitrary types of radioactive sources and camera positions. Thus, an infinite number of simulated noisy images can be generated without any additional gamma-ray irradiation tests and utilized for the robot simulator [5].

IV. EXPERIMENTS

A. Gamma-ray irradiation test

The gamma-ray irradiation test for the proposed system was conducted at the Engineering Research & Development Center of ATOX Co., Ltd. This experiment is the same experiment as the one described in [8].

Four fisheye cameras were attached to a box made of aluminum frames, as shown in Fig. 3. The camera model

TABLE I

GAMMA-RAY IRRADIATION

Camera number	Distance from ^{60}Co [m]	Air dose rate [Gy/h]
0	0.80	501
1	1.23	157
2	1.51	104
3	1.24	164

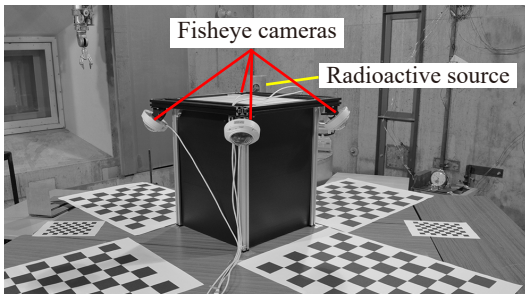

Fig. 3. Experimental settings for gamma-ray irradiation test. Four fisheye cameras were attached to the box, and a single radioactive source was placed near the cameras.

was AXIS M3007-PV, which has a FoV of 187° × 168° and supports Power over Ethernet (PoE). The camera captured images with 2592×1944 pixels at a framerate of $N_{\mathrm{fps}} = 12$.

1.0 PBq of ^{60}Co was used as the radioactive source (A = 1.0 PBq, S =^{60} Co) and placed near the cameras as illustrated in Fig. 4. The air dose rate of each camera position was measured in advance by an ionization chamber dosimeter. The results are listed in Table I.

During the irradiation test, the images captured by the cameras were stored via Ethernet in a computer placed outside the irradiation chamber. In this study, only Camera 3 was utilized to estimate the parameters for the converter module, and all four cameras were used for the comparison between the real gamma-ray image noise and the noisy images generated by the proposed method. An example image from Camera 3 is shown in Fig. 5. The red rectangular region ($W \times H = 256 \times 256$) was used to calculate the image histogram.

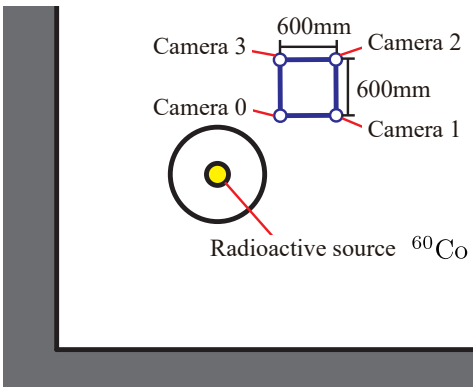

Fig. 4. Experimental layout seen from above. The radioactive source was placed near the cameras, and the room was surrounded by concrete walls.

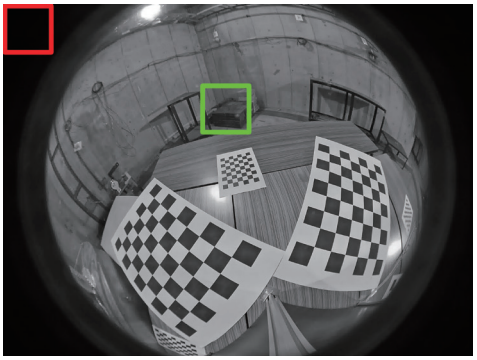

Fig. 5. Example of circular fisheye image. The region in the red rectangle was utilized for calculating the image histograms. Meanwhile, the region in the green rectangle was utilized for evaluating the proposed method. It should be noted that this image was captured before gamma-ray irradiation.

B. Monte Carlo simulation

A Monte Carlo simulation was performed based on the settings of Camera 3. The image sensor was placed in a 2.0 mm-thick aluminum box which represents the camera body. In this study, d, l_w, l_h, l_d, and l_{off} were set to 1.24 m, 1.75 µm, 1.75 µm, 7.0 µm, and 52.0 µm, respectively. Consequently, both W_{beam} and H_{beam} were set to 0.5 mm, and N_{sim} = 2,156,430 was obtained from Eq. (1).

It should be noted that when the proposed method is used for generating the simulated gamma-ray image noise for different cameras, the geometry of the cameras in the simulation should be changed according to the target cameras.

C. Parameter optimization for converter

We utilized 12 frames of the real image noise captured by Camera 3 to optimize the parameters, $\mathcal{P} \in \{p_{\mathrm{sigma}}, p_{\mathrm{Emax}}, p_{\mathrm{quality}}\}$. Here, the absolute mean error of Eq. (3) was minimized using a grid search over the parameter space $p_{\mathrm{sigma}} \in \{0.0, 0.05, \ldots, 1.0\}$, $p_{\mathrm{Emax}} \in \{1.0, 1.1, \ldots, 6.0\}$, and $p_{\mathrm{quality}} \in \{0.0, 0.05, \ldots, 1.0\}$. It should be noted that the parameters optimized using the images from Camera 3 were used to generate noisy images for all the cameras.

D. Evaluation

To evaluate the generated noisy images, we conducted a quantitative evaluation using the real image noise obtained in the gamma-ray irradiation test. We used the structural similarity (SSIM) [18] index as the evaluation metric to compare the generated noise in the images with the real image noise. Unlike the mean squared error or peak signal-to-noise ratio, SSIM evaluates the appearance similarity based on human visual perception; therefore, we hope that SSIM can properly evaluate images with spike noise. We calculated the mean value of the SSIM index for 25 frames and used the mean value as the evaluation metric.

In addition to the proposed method, noisy images were generated by a simple salt-and-pepper model for comparison. In the salt-and-pepper model, the pixel intensity of an image without noise was changed to 255 with a probability of $p_{\mathrm{sp}} \in$

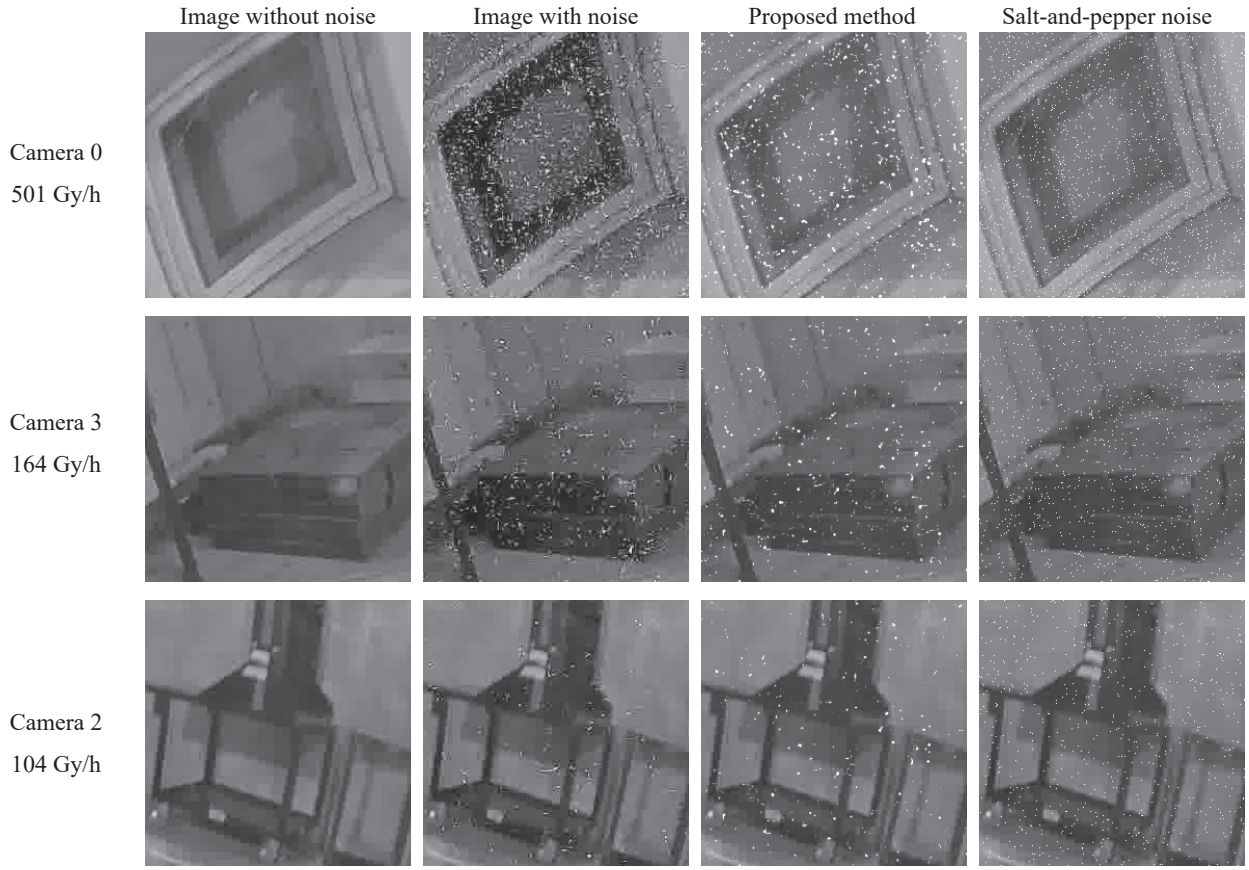

Fig. 6. Generated noisy images. From left to right: images without gamma-ray noise, images with gamma-ray noise, the noisy images generated by the proposed method, and salt-and-pepper noisy images. The camera numbers and air dose rates are shown on the left of the figure.

$[0, 1]$, where p_{sp} is a parameter that controls the amount of noise. p_{sp} was optimized using the real image noise based on image histogram comparison.

V. RESULTS

The noisy images were generated with the proposed method using the optimized parameters of $p_{\mathrm{sigma}} = 0.6$, $p_{\mathrm{Emax}} = 2.5$, and $p_{\mathrm{quality}} = 0.55$. The salt-and-pepper noisy images were generated using the optimized parameters of p_{sp} = 0.025, 0.014, 0.010, and 0.016 for Camera 0, Camera 1, Camera 2, and Camera 3, respectively.

Examples of the generated noisy images are presented along with the simple salt-and-pepper noisy images, the images without noise, and the real image noise in Fig. 6. As can be seen in Fig. 6, the proposed method generated gamma-ray image noise that is similar to the real image noise. In addition, owing to the Monte Carlo simulation, the level of image noise changes with the position of the camera. It should be noted that all the noisy images in Fig. 6 were generated based on the conversion parameters estimated using the images from Camera 3 while the parameters for the salt-and-pepper noisy images were optimized using the corresponding real-noise images. Therefore, once the parameters are estimated, the proposed method is capable of generating the gamma-ray noise of cameras placed at any position without any additional gamma-irradiation tests.

TABLE II
EVALUATION RESULTS USING SSIM INDEX ($N = 25$).

Camera number	Proposed	Salt-and-pepper
0	**0.323 ± 0.005**	0.282 ± 0.004
1	**0.584 ± 0.008**	0.490 ± 0.005
2	**0.775 ± 0.010**	0.665 ± 0.005
3	**0.589 ± 0.014**	0.456 ± 0.010

The results of the quantitative evaluation are presented in Table II, where the values in bold indicate the best scores. As can be observed in Table II, the SSIM index of the proposed method is higher than that of the salt-and-pepper model for all camera positions.

We comment on the time consumption of the proposed method. The Monte Carlo simulation took 49 s to simulate one frame in Camera 3 while the parameter optimization using a grid search consumed 216 s. These processes can be performed in advance before generating the noisy images. Once the Monte Carlo simulation and the parameter optimization have been performed, it takes 1.64 ms to generate a noisy image. Therefore, the proposed method can be combined with other simulators, such as [5].

VI. CONCLUSIONS

We proposed a novel method to simulate the image noise caused by gamma-ray irradiation. Monte Carlo simulation was utilized to calculate the interaction between the gamma-ray and the image sensor, and the energy deposit in each pixel was estimated. Moreover, we proposed a converter module that generates the image noise from the energy deposit based on image histograms.

Although real gamma-ray noise is required to optimize the conversion parameters, the proposed method can generate noisy images without an additional gamma-ray irradiation test once the parameters have been optimized. In addition, simulated noisy images with different settings can be easily generated by the proposed method, as shown in our experiments. In future work, we intend to combine the proposed method with other simulators such as [5] to add a function to generate images with noise caused by gamma-ray irradiation. We believe this study would be beneficial to the research community for the development of methods to decommission FDNPP.

ACKNOWLEDGMENT

We would like to thank Mr. Amanai, Mr. Hamada, and their colleagues from ATOX Co., Ltd., for their help and comments in the gamma irradiation test.

REFERENCES

[1] Tokyo Electric Power Company, "Roadmap on the Way to Decommissioning", https://www.tepco.co.jp/en/hd/decommission/project/roadmap/index-e.html, (Accessed 14 Aug. 2020).

[2] S. Kawatsuma, M. Fukushima, and T. Okada, "Emergency response by robots to Fukushima-Daiichi accident: summary and lessons learned", *Industrial Robot: An International Journal*, vol. 39, no. 5, pp. 428–435, 2012.

[3] K. Kawabata, "Toward technological contributions to remote operations in the decommissioning of the Fukushima Daiichi Nuclear Power Station", *Japanese Journal of Applied Physics*, vol. 59, no. 5, 050501, pp. 1–9, 2020.

[4] Japan Atomic Energy Agency, "Naraha Center for Remote Control Technology Development", https://naraha.jaea.go.jp/en/index.html, (Accessed 14 Aug. 2020).

[5] K. Suzuki and K. Kawabata, "Development of a Simulator for Underwater Reconnaissance Tasks by Utilizing Remotely Operated Robots", *Proceedings of the 2020 IEEE/SICE International Symposium on System Integration*, pp. 1100–1106, 2020.

[6] S. Nakaoka, "Choreonoid: Extensible Virtual Robot Environment Built on an Integrated GUI Framework", *Proceedings of the 2012 IEEE/SICE International Symposium on System Integration*, pp. 79–85, 2012.

[7] K. Nagatani, S. Kiribayashi, Y. Okada, K. Otake, K. Yoshida, S. Tadokoro, T. Nishimura, T. Yoshida, E. Koyanagi, M. Fukushima, and S. Kawatsuma, "Emergency Response to the Nuclear Accident at the Fukushima Daiichi Nuclear Power Plants using Mobile Rescue Robots", *Journal of Field Robotics*, vol. 30, no. 1, pp. 44–63, 2013.

[8] R. Komatsu, H. Fujii, H. Kono, Y. Tamura, A. Yamashita, and H. Asama, "Bird's-eye View Image Generation with Camera Malfunction in Irradiation Environment", *Proceedings of the 6th International Conference on Advanced Mechatronics*, pp. 177–178, 2015.

[9] E. S. Lee, G. Loianno, D. Thakur, and V. Kumar, "Experimental Evaluation and Characterization of Radioactive Source Effects on Robot Visual Localization and Mapping", *IEEE Robotics and Automation Letters*, vol. 5, no. 2, pp. 3259–3266, 2020.

[10] X. Qiao, A. Yamashita, and H. Asama, "3D Reconstruction for Underwater Investigation at Fukushima Daiichi Nuclear Power Station Using Refractive Structure from Motion", *Proceedings of the International Topical Workshop on Fukushima Decommissioning Research*, FDR2019-1006, pp. 1–4, 2019.

[11] S. Tith and N. Chankow, "Measurement of gamma-rays using smartphones", *Open Journal of Applied Sciences*, vol. 6, no. 1, pp. 31–37, 2016.

[12] T. Baca, M. Jilek, P. Manek, P. Stibinger, V. Linhart, J. Jakubek, and M. Saska, "Timepix Radiation Detector for Autonomous Radiation Localization and Mapping by Micro Unmanned Vehicles", *Proceedings of the 2019 IEEE/RSJ International Conference on Intelligent Robots and Systems*, pp. 1129–1136, 2019.

[13] S. Agostinelli, J. Allison, K. Amako, J. Apostolakis, H. Araujo, P. Arce, M. Asai et al., "Geant4—a simulation toolkit", *Nuclear instruments and methods in physics research section A: Accelerators, Spectrometers, Detectors and Associated Equipment*, vol. 506, no. 3, pp. 250–303, 2003.

[14] J. Allison, K. Amako, J. Apostolakis, P. Arce, M. Asai, T. Aso, E. Bagli et al., "Recent developments in Geant4", *Nuclear instruments and methods in physics research section A: Accelerators, Spectrometers, Detectors and Associated Equipment*, vol. 835, no. 3, pp. 186–225, 2016.

[15] S. Chauvie, S. Guatelli, V. Ivanchenko, F. Longo, A. Mantero, B. Mascialino, P. Nieminen et al., "Geant4 Low Energy Electromagnetic Physics", *Proceedings of the IEEE Symposium Conference Record Nuclear Science 2004*, vol. 3, pp. 1881–1885, 2004.

[16] K. Amako, S. Guatelli, V. Ivanchencko, M. Maire, B. Mascialino, K. Murakami, L. Pandola et al., "Validation of Geant4 electromagnetic physics versus protocol data", *Proceedings of the IEEE Symposium Conference Record Nuclear Science 2004*, vol. 4, pp. 2115–2119, 2004.

[17] Y. Rubner, C. Tomasi, and L. J. Guibas, "The Earth Mover's Distance as a Metric for Image Retrieval", *International Journal of Computer Vision*, vol. 40, no. 2, pp. 99–121, 2000.

[18] Z. Wang, A. C. Bovik, H. R. Sheikh, and E. P. Simoncelli, "Image Quality Assessment: From Error Visibility to Structural Similarity", *IEEE Transactions on Image Processing*, vol. 13, no. 4, pp. 600–612, 2004.